Fracture toughness of rotationally moulded Polyethylene and Polypropylene

Abu Saifullah[a]*, Ben Thomas[a], Robert Cripps[b], Kamran Tabeshfar[a], Lei Wang[c], Christopher Muryn[d]

[a] Bournemouth University, Talbot Campus, BH12 5BB, UK. E-mail: Thomasb@bmth.ac.uk, ktabeshf@bournemouth.ac.uk

[b] Longitude Consulting Engineers Ltd., UK. E-mail: b.cripps@longitude.uk.com

[c] Matrix Polymers, UK. E-mail: lei.wang@matrixpolymers.com

[d] School of Chemistry, Manchester University, Manchester, M13 9PL, UK. E-mail: christopher.a.muryn@manchester.ac.uk

Corresponding Author-

[a]* Abu Saifullah

Bournemouth University, Talbot Campus, BH12 5BB, UK.

E-mail: asaifullah@bournemouth.ac.uk

Fracture toughness of rotationally moulded Polyethylene and Polypropylene

Abu Saifullah[a]*, Ben Thomas[a], Robert Cripps[b], Kamran Tabeshfar[a], Lei Wang[c], Christopher Muryn[d]

[a] Bournemouth University, Talbot Campus, BH12 5BB, UK. E-mail: Thomasb@bmth.ac.uk, ktabeshf@bournemouth.ac.uk

[b] Longitude Consulting Engineers Ltd., UK. E-mail: b.cripps@longitude.uk.com

[c] Matrix Polymers, UK. E-mail: lei.wang@matrixpolymers.com

[d] School of Chemistry, Manchester University, Manchester, M13 9PL, UK. E-mail: christopher.a.muryn@manchester.ac.uk

Abstract

In this work, the fracture toughness of rotationally moulded Polyethylene (PE) and Polypropylene (PP) was measured using J integral methods at static loading rates and at room temperature. Two different commercially available rotational moulding grades PE and PP were tested in this study which have been used in various rotationally moulded products such as small leisure craft, water storage tanks etc. Scanning Electron Microscope (SEM), Optical Microscope, Differential Scanning Calorimetry (DSC), Solid-state Nuclear Magnetic Resonance (solid-state NMR) and X-ray scattering were used to investigate the microstructure, fracture surfaces and compare toughness properties of these materials. In PE, higher molecular weight and broader molecular weight distribution, larger amorphous and crystal region thicknesses are found to be related to higher toughness values. High molecular weight favours higher number of entanglements that improve fracture energy and broader distribution increases long chain branching of higher molecular weight fractions which creates higher entanglements at the branch sites. Larger amorphous regions promote micro-voiding more easily compared to thinner amorphous regions, leading to greater plastic deformation and energy absorption. Higher crystal thickness also contributes to micro-voiding in the amorphous region. For PP, greater plastic deformation observed in the fracture surfaces is related to higher fracture toughness values.

Key words: Rotational moulding, Fracture toughness, Polyethylene, Polypropylene, Microstructure.

1 Introduction

Rotational moulding is one of the fastest growing processes for the moulding of plastics due to its simplicity, stress free parts production and relatively uniform thickness distribution. This makes it particularly suitable for large, hollow plastic products [1-3]. This process consists of four stages- 1. placing the polymer powder in the mould, 2. heating with application of rotation, 3. cooling to solidify the polymer melt into the desired shape and 4. opening the mould and removal of the product [1, 3, 4]. Of the rotational grade polymers available, PE has been the most popular option for rotationally moulded products [1, 5]. Besides, there is also an increasing interest for using PP in this process.

Rotational moulding is different from other moulding processes such as injection moulding due to the zero shear [6] with prolonged heating, a long cycle time, very slow cooling rates and the presence of oxygen in contact with the mould's inner surface [1, 3]. These processing conditions create a particular morphology and microstructure that uniquely affects the mechanical behaviour of the rotationally moulded products [7, 8]. Insufficient heating causes voids or bubbles within the plastic structure due to the incomplete sintering of the powder particles and create spherulitic morphology containing very rough topography and deep gaps trapped within the polymers [8]. Overheating induces polymer degradation on the inside surfaces that is identified from the presence of carbonyl, vinyl and hydroperoxide groups in the FT-IR spectroscopy analysis. It is also evident from the viscosity changes of the degraded plastics. In the degradation of PE, viscosity is found to be increased because of the chain branching leading to chain crosslinking, whereas for the PP, it is reduced due to the chain scission [7]. The spherulitic structure is severely altered in the presence of degradation, creating small imperfect spherulites in PE and reduced cross-hatched smaller size spherulites in PP. These microstructural modifications are occurred alongside of the decrease of the melting temperature which indicates the reduction in the perfection of the crystalline structure [9, 10]. Therefore, both bubbles for the insufficient heating and degradation for the overheating are detrimental for the rotationally moulded plastics, increase the brittleness of the materials and reduce the strength. Careful monitoring of the Peak Internal Air Temperature (PIAT) during moulding cycles, using antioxidants is normally done to prevent improper heating and degradation of the polymers respectively [7, 8]. The slow cooling rate of this process increases the crystallinity and produces a larger size of spherulites in the materials leading to higher tensile and flexural properties [6], but lower impact strength with sensitivity to crack formation [7, 11]. This contrasts with injection moulding where high shear rates and rapid cooling are used to shape a product [6]. A skin-core morphology with a specific orientation is formed due to the thermo-mechanical environment applied in this process. Rapid cooling (200-500 K/min) creates smaller size spherulites with lower crystallinity.

Smaller crystalline regions and spherulites result in an increase of inter-crystalline tie molecules that improve the toughness properties of the materials [7].

In load bearing and engineering applications for both PP and PE, an improved understanding of fracture behaviour along with general strength analysis is considered necessary as it provides information on the crack growth process in the materials that can be directly relevant to their performance in real world conditions [12]. Fracture toughness measurements using different fracture mechanics approaches and the identification of crack propagation mechanisms have been investigated by previous researchers [13-29], both for PP and PE, with the research focussing on injection or other moulding processes. This type of detailed material analysis is still absent for rotationally moulded PE and PP however.

From the fracture toughness analysis of injection and compression mould grade PP it was found that the toughness is related to the initial notch depth, sample dimensions, temperature and deformation rate [13].The application of Linear Elastic Fracture Mechanics (LEFM) to measure the fracture toughness of PP homo-polymer is restricted to -60°C [14] because of the excessive non-linearity at higher temperatures [13-15]. Therefore, the elastic-plastic fracture mechanics J-integral method including multiple [16] or single specimen normalisation methods [17] and the three parameter Weibull process were used at room temperature for PP homo and co-polymers [12]. Crazing was found as the deformation mechanism for PP homo-polymer [15, 16]. For co-polymers, cavitation in the copolymer particles, shear yielding, micro-voiding and crazing were identified as the deformation mechanisms [18]. To investigate the effects of morphological parameters on fracture behaviour and toughness properties, Charpy or Izod impact strength tests have also been conducted in the literature [19, 30-32]. The crystal structure, elastomeric content present in the copolymer, molecular weight etc. are all believed to have an effect on the fracture toughness properties of PP [13, 18, 19, 30, 33-35]. The effects of annealing to achieve higher toughness in PP were investigated by previous researchers [36] . Here the fracture toughness (K_{IC}) of PE in plane strain conditions measured by following the LEFM method requires high sample size requirements especially for the high toughness grade PE [22]. Due to this limitation of LEFM, the J-integral with multiple specimen method was applied to study the fracture behaviour of high toughness grade HDPE in the range -80° C to +23° C [23]. The J-integral method was also used for LDPE and LLDPE [24]. Similarly, fracture behaviour analysis of HDPE pipes was also measured using J-integral methods in previous work [26, 27] . Analysis of both the damage zone and fracture surface was used to identify the crack growth mechanism of PE [28, 29]. Voids or micro-cracks beyond the notch region are noted to form during the application of loading to the samples, the coalescence of these voids later creates a craze ahead of the initial razor notch at $J \geq J_{IC}$ which is considered to be a crack initiation mechanism [29]. Morphological parameters such as molecular weight,

crystallinity, and the quantity and size of side chain branches were all found to have an influence on the fracture toughness properties of PE [37-41]. In addition, The rate and type of cooling of the plastic manufacturing process also changes the molecular arrangement of the polymers and this can have an effect on the fracture behaviour [38].

In this work, the fracture toughness of rotationally moulded PE and PP was measured for the first time. As detailed above, all of the current research in the literature relating to fracture toughness measurement and behaviour analysis was done for injection or other moulded PP and PE but notably not for rotationally moulded samples. By developing a better understanding of rotationally moulded PE and PP it is hoped that the potential applications for this manufacturing method can be expanded. Two different commercially available rotational moulding grades of materials for each category (PE and PP) were investigated using the elastic plastic fracture mechanics J integral method at static loading conditions at room temperature. These materials are rotationally mould grades and commonly used in various large scales, single piece plastic components such as small leisure craft hulls, oil and water storage tanks etc. An improved understanding of the fracture toughness properties and fracture behaviour analysis will help to develop safe and economical design criteria by predicting the behaviour of these rotationally moulded materials subjected to real-world external loads. Alongside the fracture toughness measurements, the microstructural arrangements of both the PE and PP grades tested were identified by using SEM, solid-state NMR, Wide and Small angle X-ray Scattering and DSC. These details were used to analyse and compare fracture behaviour, crack initiation and fracture toughness properties of the materials tested in this work under static loading conditions.

2 Experimental Methods

2.1 Material details

Two different grades of each rotationally moulded PE and PP were used in this study, supplied by Matrix Polymers Ltd. Only a limited number of material properties data is provided, listed in Table 1. Tensile stress-strain curves are presented in Figure 1 and Figure 2 for PE and PP materials respectively. Here, the PE and PP materials tested are identified as co-polymers by using Solid-state NMR, mentioned in Table 2 and described in section 3.1.1 and 3.2.1 in detail.

Table 1 Materials details[1].

Materials Grade	Materials Type	Code	MFI (g/10 min)	Density (g/cm^3)	Yield Stress (MPa)	M_w (g/mol)	M_n (g/mol)
Revolve N-307	Polyethylene-1	PE-1	3.50 *	0.939	17.7	61,080	34,660
Revolve M-601	Polyethylene-2	PE-2	3.50 *	0.949	21.5	89,400	39,970
Revolve PP-25	Polypropylene-1	PP-1	25.00**	0.902	25.5	223,800	83,600
Revolve STeQ-35	Polypropylene-2	PP-2	30.00**	0.902	23.5	212,100	40,690

[1] Data provided by the materials provider (Matrix Polymers, UK).
*Tested at 190° C and 2.16 Kg
**Tested at 230° C and 2.16 Kg

Table 2 PE and PP materials properties identified by solid state NMR and WAXS in this work.

Material Type	Material (Identified in this work as follows)	PE Content %	Side Branch Type	Side Branch Quantity (C/1000C)	Crystallinity (%)		Melting Temp. (°C)
					WAXS	DSC	
PE-1	Ethylene-1-octene co-polymer	N/A	hexyl	12	63	52.6	132
PE-2	Ethylene-1-octene co-polymer	N/A	hexyl	08	58	51.5	138
PP-1	Propylene-ethylene block co-polymer	13.4	N/A	N/A	62	47	167
PP-2	Propylene-ethylene random co-polymer	7.3	N/A	N/A	49	29	151

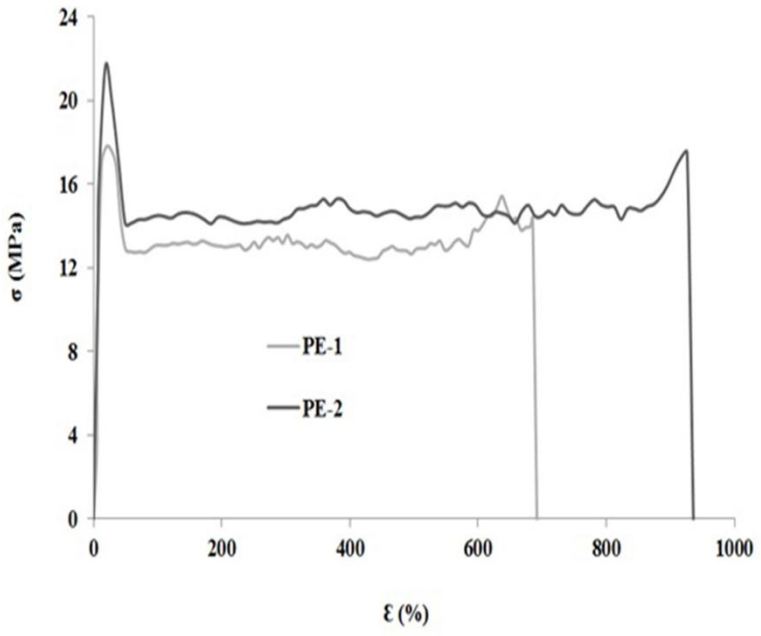

Figure 1 Tensile stress-strain curves of PE-1 and PE-2 samples.

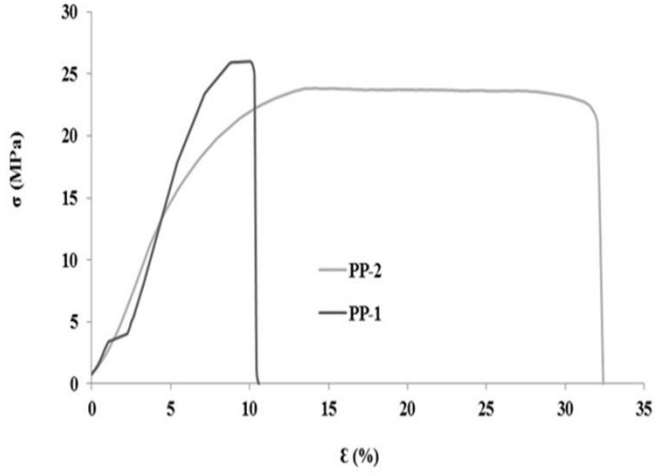

Figure 2 Tensile stress-strain curves of PP-1 and PP-2 samples.

2.2 Rotational Moulding

The rotationally moulded plastics were made using a Ferry Roto-speed Carousel type rotational moulding machine at Matrix Polymers Ltd. UK facilities. Mouldings were produced in a 300 mm steel cube mould. A shot weight of 2.5 kg was used in each trial to produce mouldings with a nominal wall thickness of 6 mm. All the mouldings were produced under the following conditions - mouldings were heated up in an oven at 300°C for 16 minutes, then the mould was removed from the oven and cooled with fans for 15 minutes and finally de-moulding was carried out.

2.3 Sample preparation

Fracture toughness tests were carried out on single edge notched bend specimens (SENB). Specimens with dimensions of 6 × 12 × 48 mm (thickness × Width × Length) were cut from the roto-moulded sheets as per the standard. An initial straight-through slot with a length to width ratio of 0.5, and terminating in a V-notch with a root radius of 0.1-0.15 mm was machined. Pre-cracks were inserted into the sample by sliding a fresh steel razor blade for every sample in the root of the machined notch to achieve a tip radius of ≤20 μm and to achieve a total crack length , a, to width, W ratio of 0.55. In Figure 3 an image of the sample is presented. A three point bending fixture was used with a span to width ratio of 4. To promote a straight crack growth, specimens were equally side-grooved.

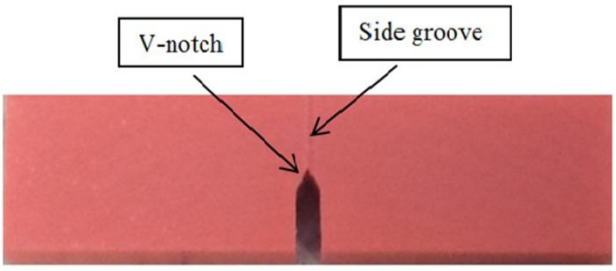

Figure 3 Test sample with v-notch and side grooves.

2.4 Fracture toughness test

The J-integral based on the multiple specimen method was used to measure the fracture toughness of the specimens by following ESIS [44] and ASTM protocols [45]. A set of identical specimens for each type of material were loaded to various displacements at a 1 mm/min crosshead speed using an Instron-8872 machine. The initial and final stable crack lengths for each specimen were measured physically from the fracture surfaces. Great care was taken during the crack length

measurements according to the standards [44, 45]. The J values were calculated from the total energy required (U) to extend the crack, which was determined from the area under the load-displacement curve obtained from the Instron-8872 data acquisition system.

$$J = \frac{2U}{B\,(W-a)} \quad (1)$$

To maintain the sample size requirements following size criteria was maintained

$$a, B, (W-a) > 25\left(\frac{J_{Ic}}{\sigma_y}\right) \quad (2)$$

Where B is the specimen thickness, W is the specimen width, a is the initial crack length, and σ_y is the yield stress of the test samples. The crack growth resistance curve (J-R) was constructed for each material tested where J was plotted against the crack extension (Δa). J_{IC} was measured at the $J_{0.2}$ position of the J–R curve.

2.5 Characterisation

Wide angle X-ray scattering (WAXS) data was collected using Bruker D8 diffractometer equipment with a sealed tube CuKα (λ = 1.54 Å) source running at 1.2 kW and collected with a lynxeye multi-strip detector. Background scattering was subtracted in order to determine the weight fraction of the crystals of each sample [36].

Small angle x-ray scattering (SAXS) measurements were performed on a HECUS SAXS/GISAXS instrument equipped with a XENOCS micro focus CuKα (λ = 1.54 Å) source with Montel optics. The diffracted X-rays were collected with a Dectris Pilatus 100K 2D detector. Thin samples (ca. 0.3mm) were cut and placed into the spectrometer at the collection position and data collected in transmission mode. Silver behenate was used for calibration of the instrument before every collection. Sample collections typically took 4000 seconds. Irena SAS/SANS routines (S1) in Wavemetrics Igor Pro have been used for calibration, data conversion and subsequent analysis [42]. The lamellar long period, D, lamellar thickness (L_c) and volumetric percentage of crystallinity (x_{vol}) were also calculated [43].

Differential scanning calorimetry (DSC) was done with a METTLER TOLEDO DSC 823e instrument, placing 5-7 mg samples in an aluminium pan and heated from 40 to 200°C at the rate of 10° C/min under a continuous nitrogen purge. The heat required for melting (ΔH) was measured by integrating the area under melting peak of each sample. The degree of

crystallinity was calculated by dividing the heat required for melting (ΔH) of different treated materials by the heat required for melting a 100% crystalline sample (ΔHC). For PE, ΔHC = 293.6 J/g [44] and for PP, ΔHC = 209 J/g [45] were taken.

Solid state ^{13}C nuclear magnetic resonance (Solid-state NMR) spectra were acquired using a Varian VNMRS spectrometer operating at 100.56 MHz for identifying the details of polymer structure of the plastics, side chain branches and quantity of the co-monomers used in PP and PE, using a 6 mm (rotor outside diameter) magic-angle spinning (MAS) probe. Spectra from PE and PP samples were obtained with both cross-polarisation (CP) and single-pulse excitation (SPE) MAS at room temperature with a spinning frequency of 6 KHz. CP spectra were recorded with a recycle delay of 2 s and contact time of 1 ms. Quantitative SPE spectra were acquired using a 90° pulse of 4.5 μs and a 60 s recycle delay to ensure complete relaxation of the ^{13}C nuclei. These spectra were referenced to tetramethylsilane (Me_4Si) by sitting the isotropic high-frequency peak of adamantane to 38.56 ppm.

An Optical microscope (VHX-5000) was used to identify the real crack front and to measure the crack length on the fracture surfaces. Scanning electron microscope (SEM) (JEOL, JSM-6010 PLUS/LV) images were taken at different magnification scales after applying 50 seconds gold coating for every specimen with an Agar auto sputter-coater gold coating instrument.

3 Results and Discussion

3.1 Polyethylene (PE)

3.1.1 WAXS, SAXS, DSC, Solid-state NMR Analysis

Figure 4 shows similar groups of peaks in the 20-30 [°2θ] scattering angle regions of the WAXS curve for both of the PE materials. These peaks represent the (110) and (200) crystal planes that confirm the orthorhombic crystal in PE-1 and PE-2 as well [46, 47]. The crystallinity was calculated and listed in Table 2.

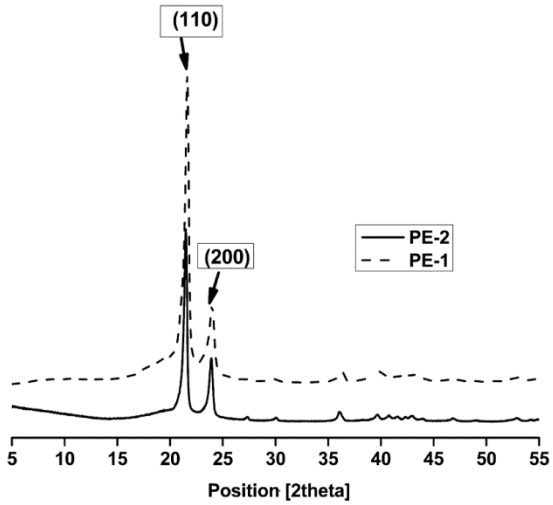

Figure 4 Crystal structures of PE-1 and PE-2 from WAXS analysis.

Long period (D), crystal and amorphous thickness (L_C and L_a) of PE materials were measured from the q values shown in Figure 5 and shown in Table 3. PE-2 is shown to have a higher long period than PE-1. Moreover, higher crystal and amorphous region thickness was also found for PE-2. This matches the higher crystal thickness also found for PE-2 in the DSC analysis due to the increased melting temperature.

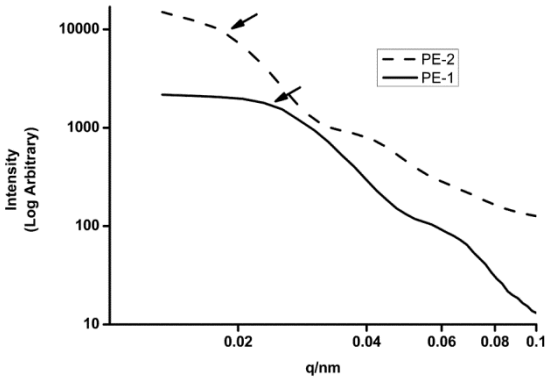

Figure 5 1-D SAXS curves of PE-1 and PE-2.

The melting point and crystallinity were measured for PE-1 and PE-2 from the DSC curves (Figure 6), as per Table 2. Only one peak was found in their DSC curves, representing the same type of crystal – orthorhombic phase that was also found in the WAXS analysis. Crystallinity measured for both PE-1 and PE-2 in DSC analysis showed lower value than that of in WAXS analysis. Lower crystallinity in DSC analysis compared to WAXS analysis was also observed by Isasi et al.[48]. They concluded that in the DSC analysis only core crystallinity is measured while both the core crystallinity and interfacial

region are measured in WAXS analysis. Because of this WAXS analysis always shows higher crystallinity than that of DSC analysis. PE-2 showed very close crystallinity to PE-1, less by only one percent in DSC analysis whereas PE-2 showed five percent less crystallinity compared to PE-1 in WAXS analysis. PE-2 was found to be shown the higher melting point at 137°C due to the higher long period and crystal thickness measured in SAXS analysis and density compared to PE-1. No reason was identified for the lower crystallinity of PE-2 in this work.

Table 3 Quantitative SAXS information for microstructure of PE and PP.

Materials	**Long period (crystal + amorphous region) (A°)**	**Crystal thickness (A°)**	**Amorphous thickness (A°)**
PE-1	191.88	113.20	78.67
PE-2	309.27	167.00	142.26
PP-1	181.30	108.05	73.24
PP-2	142.10	54.50	87.60

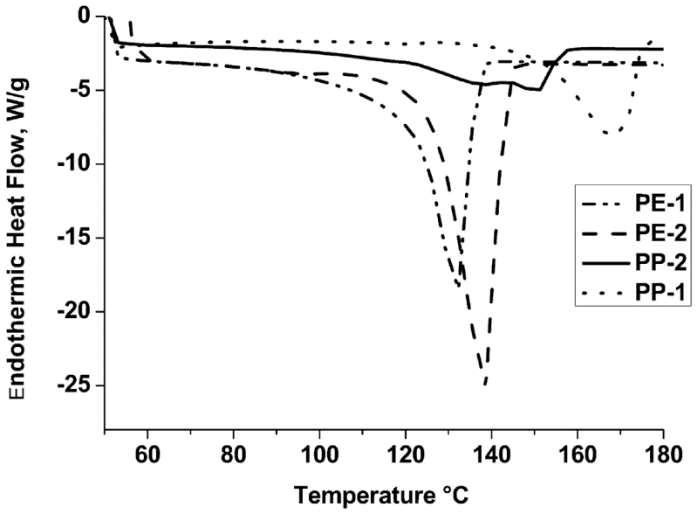

Figure 6 DSC curves of melting behaviour for PE and PP tested in this study.

In Figure 7 intense sharp peaks at ppm 32.9 and 31 were clearly seen in solid-state carbon-13 NMR single pulse excitation (SPE) spectra for the orthorhombic crystalline phase and amorphous region respectively [49-51] for the both PE materials. In addition, a second peak was also observed at ppm 14.9 for PE 1 and PE-2. This corresponds to hexyl side branches present in the microstructure [49, 51]. In PE, copolymerisation is used to improve the density and ultimate material

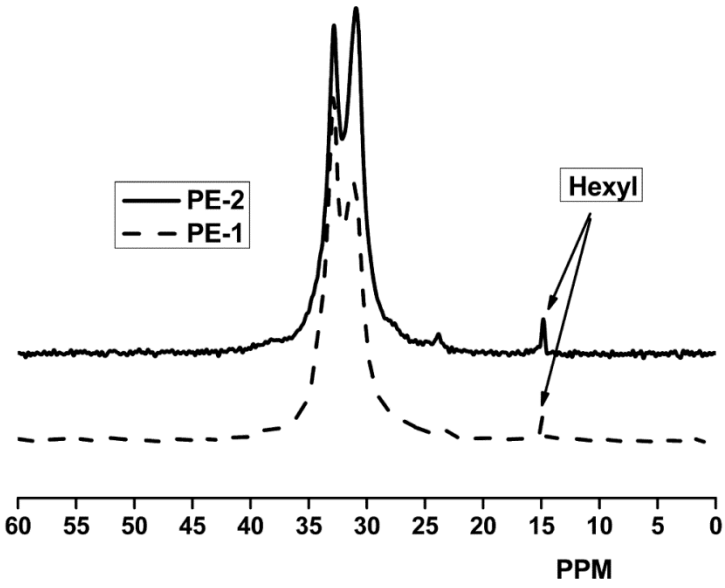

Figure 7 Solid State SPE MAS spectra of PE-1 and PE-2.

properties. Co-monomer 1-octene introduces hexyl side branches in the PE main chain and this explains the additional peak seen in the NMR analysis. Therefore, it can be said that the rotational grade PE-1 and PE-2 materials tested are ethylene-1-octene copolymers. De-convolution of the SPE spectra provides the quantitative information on side chain branching in PE. The quantity of side branches is listed above in Table 2. In general, higher branching acts to decrease the density of PE, this matches our observations here as PE-2 showed the highest density and the lowest number of side branches (8 C/1000C).

3.1.2 Fracture Toughness and Fractography

Fracture toughness ($J_{0.2}$) values were calculated from the J-R curves for PE-1, PE-2 (see Figure 8) and shown below in Figure 9. The J-R curve is found to follow the power law relation $J = A\,(\Delta a)^N$, N≤1 and confirms the plane strain state fracture condition according to equation no. 2. PE-2 is seen to have higher fracture toughness values than that of PE-1, though they are close to each other. Figure 10 shows the low magnification images (a, b) and the scanning electron microscope images (c, d) of the fracture surfaces of PE-1 and PE-2 and confirms the differences of fracture toughness values between PE-1 and PE-2. Three distinct zones were clearly identified on the surfaces (Figure 10- a, b), the stress whitened slow stable crack growth zone (Z-1), the diffuse and smooth stress whitened zone for plastic deformation (Z-2) and the brittle fracture zone (Z-3). Higher magnification SEM images (Figure 10 - c, d) of Z-1 for all the PE's tested reveal microfibrillar morphology during loading which is seen to be more extensive for PE-2. In PE, voids are observed to form next to the notch region under load. These voids create crazes as they coalesce leading to fibril formation and subsequent

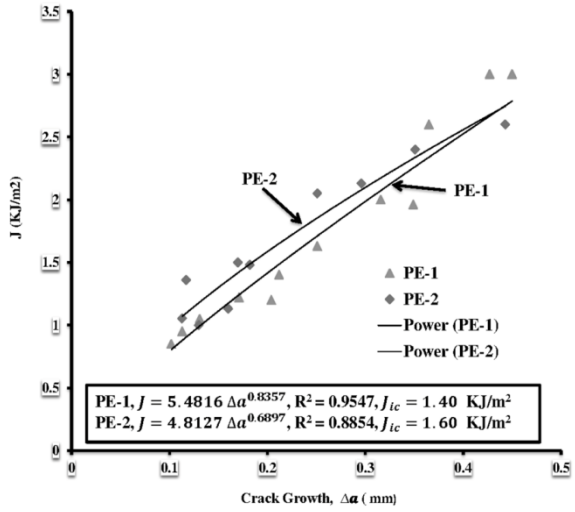

Figure 8 J-R curve of PE-1and PE-2.

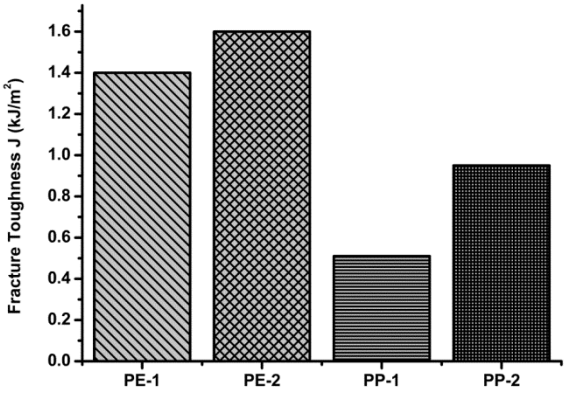

Figure 9 Fracture Toughness values of PP and PE samples at $J_{0.2}$ in J-R curve.

rapid crack propagation [29, 52]. This more extensive microfibrillar morphology leads to more plastic deformation and higher fracture toughness in PE-2 over PE-1 tested here. This is because more energy is needed to break these fibrils in order to start the rapid crack propagation. In Z-3, stick-slip lines were seen under the optical microscope for both of the PE materials tested, these are characterised by protuberant ridges (R). These ridges slow down the crack growth in the rapid crack growth region [28, 52]. Three ridges were observed in PE-2, with two ridges seen for PE-1. For PE, different fracture toughness values are found in the published research works for other moulding processes depending on their composition and toughness grade. Swei et al. [29] tested different grades of PE at room temperature and reported 1.7 kJ/m^2 and 8.2 kJ/m^2 as J_{IC} values for HDPE and gas pipe grade tough PE copolymer respectively. Microfibrillar tufts and dimple-like

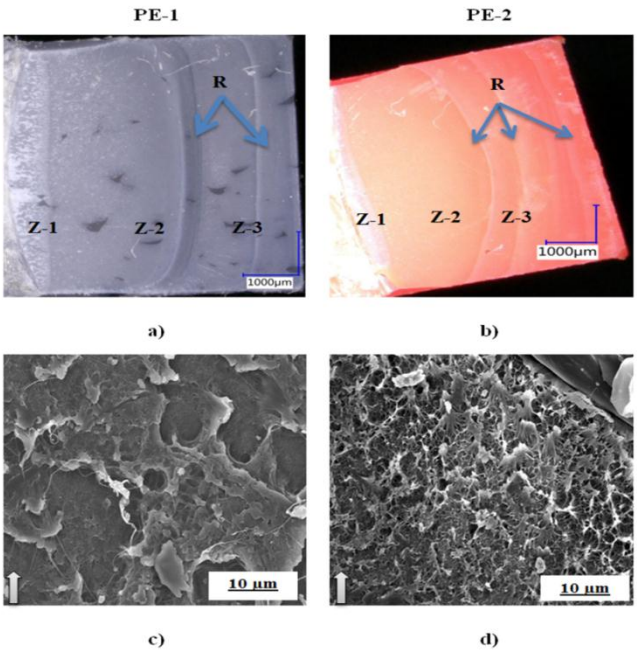

Figure 10 Fracture surfaces under optical microscope of (a) PE-1, (b) PE-2 and SEM images (c) PE-1 (d) PE-2 taken at Zone-1 (z-1).The arrow indicates the crack growth direction.

characteristics were identified in the slow crack growth region which is also found in this work. For conventional HDPE a 1 kJ/m^2 J_{IC} value was reported [22]. Several extrusion moulded pipe grade HDPEs were found to have J_{IC} values in the range of 0.2 kJ/m^2 to 20 kJ/m^2 at room temperature depending on their strain rate in the testing process [53]. For tough grade compression moulded HDPE and pressurised HDPE pipe using in gas or water distribution 28 kJ/m^2 and 31 kJ/m^2 fracture toughness values were measured at 23 °C respectively [23, 54]. In this work fracture toughness values for rotationally moulded PE are lower particularly compared to high tough grade extrusion , compression or gas pipe PE, though there are differences between the PE materials. The differences in fracture toughness can be attributed to material compaction as rotational moulding is a low pressure method compared to extrusion, compression and injection molding.

3.2 Polypropylene (PP) results

3.2.1 WAXS, SAXS, DSC and Solid-state NMR Analysis

WAXS was performed on both PP-1 and PP-2 samples and showed the peaks with some differences in peak intensity and peak position (Figure 11). Three main peaks at 2θ scattering angles of (13.92), (16.74) and (18.42) were observed in PP-1, these represent diffraction from the crystallographic planes of 110, 040 and 130 respectively for the α crystal form of PP [33, 55-57]. In PP-2, the intensity of these three peaks is seen to be reduced particularly for the (130) plane peak at 18.42 [°2θ]

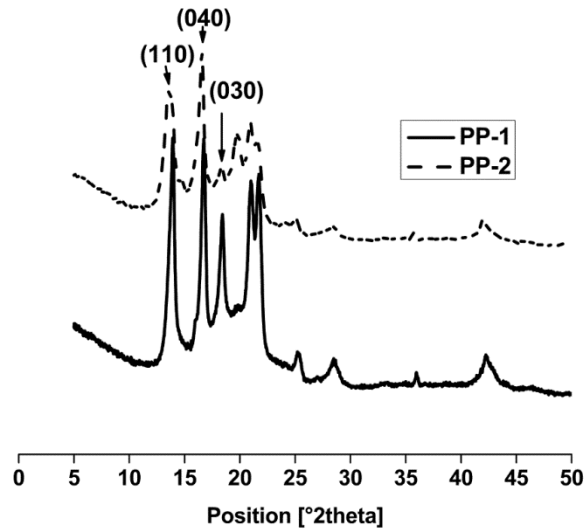

Figure 11 Crystal structure of PP-1 and PP-2 measured in WAXS.

scattering angle. A Peak at 20 [°2θ] scattering angle was observed for PP-2 for the (117) crystal plane that corresponds to the γ polymorph in the PP [45]. The γ form was found for low molecular weight isotactic PP and random copolymers of propylene and α-olefins [58]. The crystallinity was calculated and listed in Table 2. The crystallinity ratio was found to be lower for PP-2. Figure 12 represents the one- dimensional SAXS results for both types of PP tested. PP-2 is seen to have a lower crystal and higher amorphous thickness than that of PP-1(Table 3).

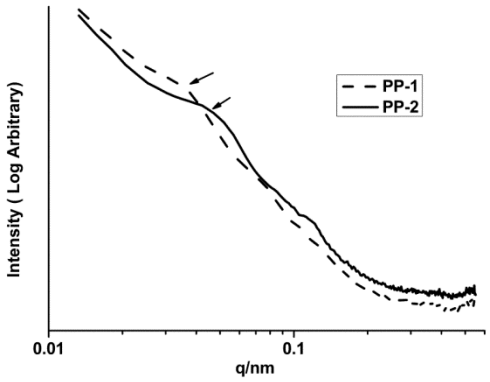

Figure 12 SAXS 1-D curves of PP-1 and PP-2 materials.

The DSC (Figure 6) curves for PP-1 shows the thermal behaviour only for the α-crystal phase. A doubling or shoulder melting peak was observed for the α and γ-crystal phase in the DSC graphs for PP-2 [45] which also supports the WAXS profiles. Crystallinity was also measured in DSC analysis. It was found that both PP-1 and PP-2 showed lower crystallinity in DSC analysis compared to WAXS analysis, mentioned in Table 2. Because in DSC analysis only core crystallinity is

measured whereas in WAXS analysis both core crystallinity and interfacial region are measured [48]. The melting temperature of PP-2 was found to be lower than that of PP-1, this could be due to the lower crystallinity observed in DSC and WAXS analysis in this study [34, 59].

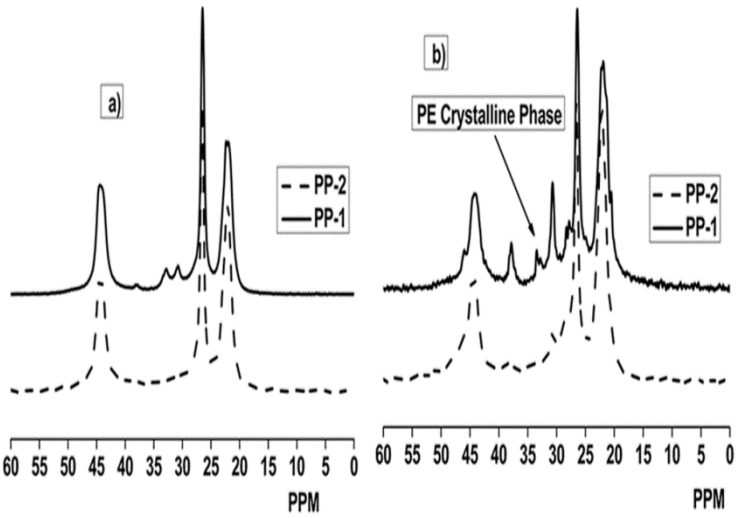

Figure **13** (a) 13C CP and (b) SPE MAS NMR spectrum of the PP-1 and PP-2 samples performed at room temperature. A recycle delay of 60 s was applied for SPE spectra.

From the CP/MAS (cross polarisation/magic angle spinning) spectra (Figure 13-a), signals at 44 and 22 ppm in the methylene (-CH_2-) and methyl region were observed, confirming that these PP materials are isotactic PP [60]. The methine (-CH-) carbon showed a peak at 26.5 ppm for both PP materials, this represents the crystalline phase. Other signals were also found at 31 and 33 ppm for PP-1 which were not observed for PP-2 in CP/MAS spectra. Peaks at 31 and 33 ppm represent the amorphous and crystalline PE phase in the PP matrix respectively [61]. SPE (Figure 13-b) was used to provide quantitative information for all regions. For PP-1, peaks at 31 and 33 ppm were identified whereas the peak at 33 ppm was not observed for PP-2. Prasad [62] identified a signal at 33 ppm for the block copolymers of propylene with ethylene which was not observed for random propylene-ethylene copolymers. Botha et al. [61] also observed a peak at 33 ppm for block propylene ethylene copolymers. In the SPE spectra a signal at 38 ppm was also observed for both PP-1 and PP-2, this is reported as the best resonance for the quantification of the ethylene phase or defects in the propylene- ethylene copolymers [61, 63]. The ethylene content was quantified from the de-convolution of the SPE spectra as per Table 2. From these results, it can be said that PP-1 and PP- 2 are propylene-ethylene block and random copolymers with 13.4 % and 7.3 % PE content respectively.

3.2.2 Fracture Toughness and Fractography

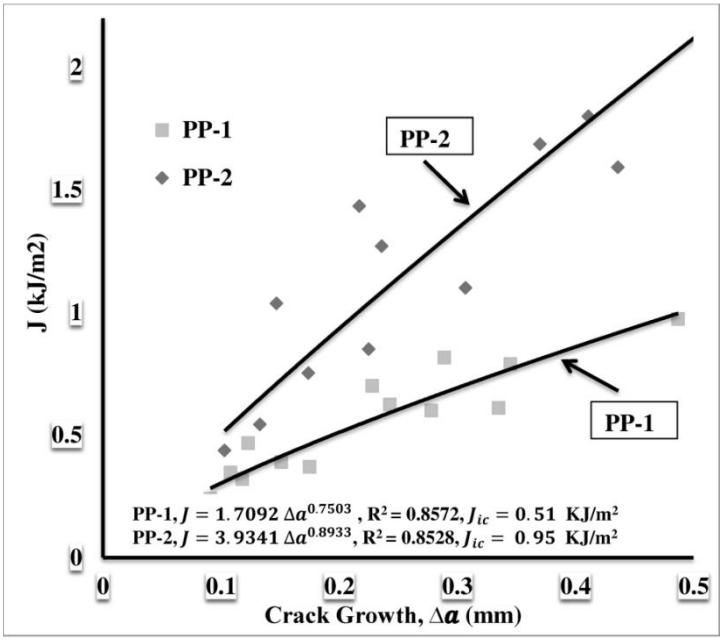

Figure 14 J-R crack growth resistance curves for PP-1 and PP-2.

Figure 14 provides the J-crack growth resistance curve (J-R) curve of PP-1 and PP-2. This plot also includes the fit of the J-R curve to the power law $J = A\ (\Delta a)^N$, N≤1. Fracture toughness $J_{0.2}$ values of PP-1 and PP-2 are presented in Figure 9. It was found that PP-2 has almost double the fracture toughness as the PP-1 material. These fracture toughness values followed the plane strain state, confirmed from equation 2. The fracture toughness values measured in this work for PP-1 and PP-2 are very low compared to those published in literature for other manufacturing methods such as injection moulding process. In injection moulding process 19 kJ/m^2 and 9 kJ/m^2 were reported for the PP random and block co-polymers respectively as fracture toughness values [13]. It must be noted that the materials tested in injection moulding process differ in composition from the PP random and block co-polymer (PP-1 and PP-2 respectively) tested in this work. Different moulding processes are required different grade of materials and the plastics are manufactured under different processing conditions and hence mechanical properties are changed in the plastics. Rapid cooling of injection moulding process induces lower crystallinity and small spherulites that increase the toughness property. Rotational moulding is a low pressure method compared to injection, compression or extrusion moulding. Besides, the absence of shear and the low cooling rates in rotational moulding process favour the coarse, larger and brittle spherulitic morphology in PP that reduces the impact toughness found in previous research work [64]. This could be a reason for the observed lower fracture toughness of rotationally moulded PP materials tested in this work. Three different zones were observed on the fracture surfaces (Figure 15) for both of the PP

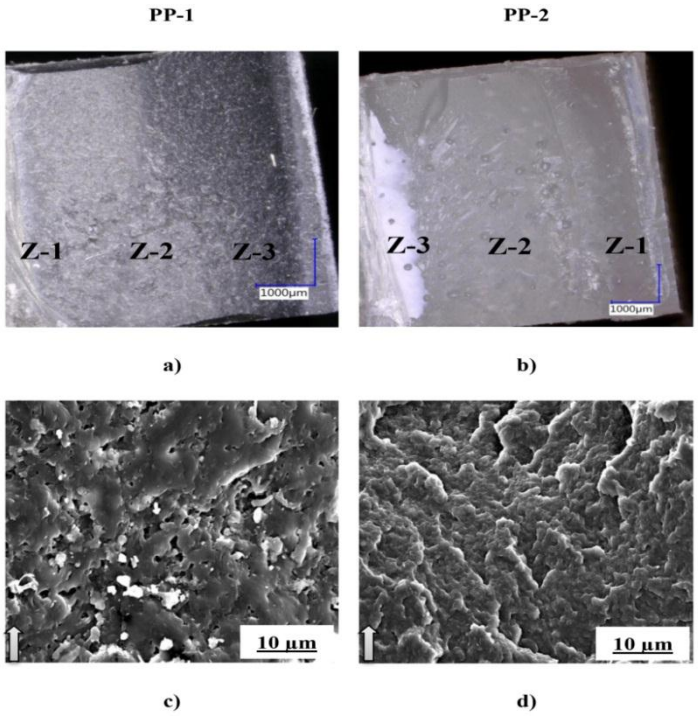

Figure 15 Fracture surface (a, b) under optical microscope and SEM images (c, d) of PP-1 and PP-2 respectively at Zone -1. The arrow points out the crack growth direction.

materials using the optical microscope. In PP-2, a deep stress whitened area is situated next to the notch (Z-1), after that a large, diffuse, smoother stress whitened area is noted as Zone-2 (Z-2) and finally, an un-whitened and plain area is found as Zone-3 (Z-3). PP-1 also shows these different regions, however there is less depth of stress whitened area in Zone-1. These three zones were also observed in previous studies by various researchers for PP, here, Zones 1, 2 and 3 were described as an outcome of slow stable crack growth , plastic deformation and brittle fracture respectively [13]. In general, crazing is the main deformation process for PP, crazes appear and develop around the crack tip and proceed up to a certain point beyond which they can't go further and this finally leads to rapid brittle fracture. No shear leap was found in any of the materials tested. Some deflected crack paths were observed in PP-2, which could be due to small voids generated during the manufacturing process in the fracture surfaces or due to shear yielding, which was also reported in previous research work [13, 65]. Under the SEM, Figure 15 (c, d), PP-1 shows the flat and smooth surfaces that are related to brittle fracture with lower plastic deformation, whereas for PP-2 the surfaces are wavy and patchy, with micro-voiding due to the de-bonding between the PP matrix and PE phases. For PP-2 Micro-voiding, wavy or patchy-like structures that act to increase plastic deformation with increasing ductility and fracture toughness values [55] were observed.

3.3 Discussion

In this work, it was confirmed that the rotational mould grade PE-1 and PE-2 materials tested are ethylene-1-octene copolymers based on the solid-state NMR and WAXS analyses. From the SAXS and J-R curves, PE-2 was found to have higher amorphous and crystal thickness as well as higher fracture toughness for the two PE materials tested. PE-2 also showed lower crystallinity than PE-1 both in DSC and WAXS analysis. For the fracture toughness analysis and slow crack growth process, crystallinity is not the main governing factor [38] and toughness value was found to be decreased with the increase of crystallinity as higher crystallinity induces comparatively more brittle behaviour, reduction in craze formation and amorphous region [66]. From Table 1 it is found that PE-2 has higher molecular weight and broader molecular weight distribution compared to PE-1 which are related to higher fracture toughness of PE-2. Because high molecular weight favours the higher number of entanglements among the tie chains connecting lamellar blocks leading to greater plastic deformation with higher fracture energy absorption [37] and broader molecular weight distribution results in an increase in long chain branching of higher molecular weight fractions which create higher degree of entanglements at the branch sites [67]. Higher amorphous and crystal thicknesses are also responsible for the higher toughness value seen in PE-2. The toughening mechanism due to the higher amorphous thickness was described in recent research works [36, 68]. For higher amorphous region thickness in PE-2, more flexible chain structures are created in the amorphous phase. The flexible amorphous region makes the formation of the micro-voiding process easier which has a positive effect on fracture toughness. Easier formation of micro-voids that help to increase crazing leads to more fibril formation, and more energy absorbed (Figure 10 - c, d) for crack growth initiation and propagation which accounts for the higher fracture toughness of this material. The higher crystal thickness measured in PE-2 results in better crystal perfection [52]. The perfection of the crystals contributes to the micro-voiding process in the amorphous region , enhances plastic deformation with more absorbed energy before crystallite shearing, resulting in higher toughness [68].

From the WAXS analysis, it was found that in the crystalline region PP-1 has α crystal structure whereas PP-2 contains both α and γ polymorph in its crystal structure. Solid state NMR analysis confirmed PP-1 and PP-2 as propylene-ethylene block and random copolymers respectively. It is found that PP-1 has a higher molecular weight and narrow molecular weight distribution (Table 1) compared to PP-2. Linear relationship between molecular weight and fracture energy was not observed for PP-1 here. This could be due to its narrow molecular weight distribution since narrow molecular distribution needs to have very high molecular weight to achieve the same level of toughness of broad molecular weight distribution [67]. Here, PP-2 has a larger amorphous thickness and showed better fracture toughness with values recorded almost double

that of PP-1 in this work. A higher amorphous thickness absorbs more energy for crack initiation and propagation [36, 68]. Though PP-2 is seen to have a larger amorphous thickness and better fracture toughness compared to PP-1, it is difficult to directly compare fracture toughness between PP-2 and PP-1 based on microstructural details as they have different chemical composition in their structure. In PP-2, the γ crystal form increases the energy absorption and resistance to deformation [69, 70]. The γ crystal form only shows transverse slip in its chain arrangement instead of slip along the chain direction during the deformation or crack growth process as it does not contain any parallel chain arrangement. Transverse slip absorbs more energy and shows higher resistance to deformation. In this work, SEM images show brittle and plastic deformation for PP-1 and PP-2 in the fracture surfaces respectively. Plastic deformation absorbs more energy and tends to increase toughness values [55] and this was observed for PP-2 in this work.

The fracture toughness values measured in this work for PE and PP materials are very low, notably lower for PP compared to those published in the literature, though they differ in composition from the PP and PE materials investigated in this study. Differences in rotational and various moulding processes might be a reason for this.

4 Conclusions

The following conclusions can be drawn from the fracture toughness measurement analysis of rotationally moulded PP and PE, conducted in this work.

- PE-1 and PE-2 were identified as ethylene-1-octene copolymers with same side chain length. Higher molecular weight and broader distribution, thicker amorphous and crystal region in PE-2 are the reasons for its better fracture toughness value over PE-1. High molecular weight and broader distribution increase the number of entanglements that improve fracture energy. The thicker amorphous region contains flexible chain structures which create easier micro-voids formation, absorbing more energy and resulting in increased toughness values. Greater perfection of the crystals within the higher crystal thickness also contributes to micro-voiding in the amorphous region before crystallite shearing occurs and enhances toughness.
- PP-1 and PP-2 are block and random propylene-ethylene copolymers. Though PP-1 has higher molecular weight, it shows lower fracture toughness compared to PP-2 as it has narrow molecular weight distribution. PP-2 contains a higher amorphous thickness and both α and γ crystal structure whereas PP-1 has thinner amorphous region and only α crystal structure. The γ crystal structure increases the resistance to deformation. Greater plastic deformation is

evident in the fracture surfaces for PP-2 and increases toughness values. Brittle type failures in PP-2 are also reflected into less deformation ability with lower toughness values.

- Fracture toughness values measured in this work are lower than those recorded for other moulding processes in the literature which could be due to the unique characteristics of rotational moulding process.
- The findings of this work provide a better understanding about the suitability and fracture behaviour of these tested materials subjected to real-world external static loads and it is hoped this increased understanding will widen the range of potential applications for rotationally moulded components.

Acknowledgements

We express our sincere thanks to Matrix Polymer and FJ Engineering for the rotary moulding of the plastics and test samples development. We also wish to gratefully acknowledge the support from the EPSRC UK National Solid-state NMR service at Durham University, UK and to the University of Manchester, UK for conducting the solid-state NMR and SAXS, WAXS characterisation of the materials respectively.

References

1. R.J. Crawfoard and M.P. Kearns, *Introduction to the Rotational Moulding Process*. *In: Practical guide to rotary moulding* (2003), Shrewsbury.
2. F. Torres and C. Aragon, *Polymer Testing*, **25**, 568 (2006).
3. R.J. Crawfoard, *Journal of Materials Processing Technology*, **56**, 263 (1996).
4. M. Cramez, M. Oliveira and R.J. Crawfoard, *Polymer Degradation and Stability*, 2002. **75**, 321 (2002).
5. S. Waigaonkar, B. Babu and R.D. Prabhakaran, *Journal of Reinforced Plastics and Composites*, **27**, 1021 (2008).
6. J. Godinho, A. Cunha and R.J. Crawfoard, *Proceedings of the Institution of Mechanical Engineers, Part L: Journal of Materials Design and Applications*, **216**, 179 (2002).
7. M. Oliveira and M. Cramez, *Journal of Macromolecular Science Part B*, **40**, 457 (2001).
8. M. Oliveira, M. Cramez and R.J. Crawfoard, *Journal of materials science*, **31**, 2227 (1996).
9. B. Terselius, U.W. Gedde and J-F. Jansson, *Polymer Engineering & Science*, **22**, 422 (1982).
10. U.W. Gedde, J-F. Jansson and B. Terselius, *Polymer Engineering & Science*, **27**, 427 (1987).
11. K. Friedrich, *Kunststoffe-German Plastics*, **69**, 796 (1979).
12. B.L. Shao-Yun Fu and M. Yiu-Wing, *Fracture Mechanics*, in *Science & Engineering of short fibre reinforced polymer composites*, USA, 231 (2009).
13. A. Salazar, P. Frontini and J. Rodríguez, *Engineering Fracture Mechanics*, **126**, 87 (2014).
14. P. Fernando and J. Williams, *Polymer Engineering & Science*, **20**, 215 (1980).
15. E. Santarelli and P. Frontini, *Polymer Engineering & Science*, **41**, 1803 (2001).
16. A. Salazar, J. Rodríguez and A. Martínez, *Engineering Fracture Mechanics*, **101**, 10 (2013).
17. C. Morhain and J. Velasco, *Journal of materials science*, **36**, 1487 (2001).
18. L.A. Fasce, *Journal of Polymer Science Part B: Polymer Physics*, **42**, 1075 (2004).
19. L. Fasce, V. Pettarín, C. Bernal and P. Frontini, *Journal of Applied Polymer Science*, **74**, 2681 (1999).
20. D. Ferrer-Balas, M.L.s. Maspoch, and Y.-W. Mai, *Polymer*, **43**, 3083 (2002).
21. Y.-W. Mai and B. Cotterell, *International Journal of Fracture*, **32**, 105 (1986).
22. M. Chan and J. Williams, *Polymer Engineering & Science*, **21**, 1019 (1981).
23. M. Chan and J. Williams, *International Journal of Fracture*, **23**, 145 (1993).
24. S. Hashemi and J. Williams, *Polymer*, **27**, 384 (1986).

25. A. Pegoretti, L. Castellani, L. Franchini, P. Mariani and A. Penati, *Engineering Fracture Mechanics,* **76**, 2788 (2009).

26. T.M.A.A. EL-Bagory, H.E.M. Sallam and M.Y.A. Younan, *Theoretical and Applied Fracture Mechanics,* **74**, 164 (2014).

27. A. Benhamena, L. Aminallah, B.B. Bouiadjra, M. Benguediab, A. Amrouche and N. Benseddiq, *Materials & Design,* **32**, 2561 (2011).

28. M. Chan and J. Williams, *Polymer*, **24**, 234 (1983).

29. H. Swei, B. Crist and S. Carr, *Polymer*, **32**, 1440 (1991).

30. Z. Sun and F. Yu, *Die Makromolekulare Chemie,* **192**, 1439 (1991).

31. J. Jancar, A. DiAnselmo, A.T. DiBenedetto and J. Kucera, *Polymer,* **34**, 1684 (1993).

32. P. Doshev, R. Lach, G. Lohse, A. Heuvelsland, W. Grellmann and H-J. Radusch, Polymer, **46**, 9411 (2005).

33. E. Nedkov and T. Dobreva, *European Polymer Journal,* **40**, 2573 (2004).

34. H.B. Chen, J. Karger-Kocsis, J.S. Wu and J. Varga, *Polymer,* **43**, 6505 (2002).

35. H. Du, Y. Zhang, H. Liu, K. Liu, M. Jin, X. Li and J. Zhang, *Polymer,* **55**, 5001 (2014).

36. C. Geng, G. Yang, H. Bai, Y. Li, Q. Fu and H. Deng, *The Journal of Supercritical Fluids,* **87,** 83 (2014).

37. M. Wang, E. Nakanishi and S. Hibi, *Polymer,* **34**, 2792 (1993).

38. X. Lu, R. Qian and N. Brown, *Polymer*, **36**, 4239 (1995).

39. B. Crist, C.J. Fisher and P.R. Howard, *Macromolecules,* **22**, 1709 (1989).

40. A.R. Wolfe, *Plastics Pipes X: Plastics Pipeline Systems for the Millennium, Conference Papers,* (1998).

41. P. Gupta, G.L. Wilkes, A.M. Sukhaida, R.K. Krishnaswamy, M.J. Lamborn, S.M. Wharry, C.C. Tso, P.J. Deslauriers, T. Mansfield and F.L. Beyer, *Polymer,* **46**, 8819 (2005).

42. J Ilavsky and P.R. Jemian, *J. Appl. Cryst*., **42**, 347 (2009).

43. B.A.G. Schrauwen, R.P.M. Janssen, L.E. Govaert and H.E.H. Meijer, *Macromolecules,* **37**, 6069 (2004).

44. S.L. Kodjie, L. Li, B. Li, W. Cai, C.Y. Li and M. Keating, *Journal of Macromolecular Science, Part B: Physics*, **45**, 231 (2006).

45. M.L. Cerrada, E. Pérez, R. Benavente, J. Ressia, C. Sarmoria and E.M. Vallés, *Polymer Degradation and Stability*, **95**, 462 (2010).

46. R. Pereira, E. Mano and M. Dias, *Polymer Testing*, **16**, 589 (1998).

47. E.L. Heeley, D.J. Hughes, Y. El. Aziz, P.G. Taylor and A.R. Bassindale, *European Polymer Journal,* **51**, 45 (2014).

48. J.R. Isasi, L. Mandelkern, M.J. Galante and R.G. Alamo, *Journal of Polymer Science Part B: Polymer Physics*, **37**, 323 (1999).

49. X. Gao, L. Wang, H. Luo, Q. Zou, N. Feng and J. Feng, *Macromolecules*, **43**, 5713 (2010).

50. M. Wang, G.M. Bernard, R.E. Wasylishen, P. Choi, *Macromolecules*, **40**, 6594 (2007).

51. M. Pollard, K. Klimke, R. Graf and H.W. Spiess, *Macromolecules*, **37**, 813 (2004).

52. Z.M. Li, Z.Q. Qian, M.B. Wang, Y. Wang, B.H. Xie and R. Huai, *Polymer*, **46** , 10466 (2005).

53. D. Barry and O. Delatycki, *Polymer*, **33**, 1261 (1992).

54. A. Salazar, J. Rodríguez, F. Arbeiter and G. Pinter, *Engineering Fracture Mechanics*, **149**, 199 **(**2015).

55. Y. Shao, C. Wu, S. Cheng, F. Zhou and H. Yan, *Polymer Testing*, **41**, 252 **(**2015).

56. E. Lezak, Z. Bartczak and A. Galeski, *Polymer*, **47**, 8562 (2006).

57. A. Weidinger and P. Hermans, *Die Makromolekulare Chemie*, **50**, 98 (1961).

58. E. Pérez, D. Zucchi, M.C. Sacchi, F. Forlini and A. Bello, *Polymer*, **40**, 675 (1999).

59. J. Varga, *Journal of Macromolecular Science, Part B*, **41**, 1121 (2002).

60. A. Comotti, R. Simonutti, S. Bracco and L. Castellani, *Macromolecules*, **34**, 4879 (2001).

61. L. Botha, P. Sinha, S. Joubert and H. Duveskog, *European Polymer Journal*, **59**, 94 **(**2014).

62. J. Prasad, *Journal of Polymer Science Part A: Polymer Chemistry*, **30**, 2033 (1992).

63. R.G. Alamo, A. Ghosal, J. Chatterjee and K.L. Thompson, *Polymer*, **46,** 8774 (2005).

64. M. Cramez, M. Oliveira and R.J. Crawford, *Journal of Materials Science*, **36**, 2151 (2001).

65. R. Gensler, C.J.G. Plummer, C. Grein, H.H. Kausch, *Polymer*, **41**, 3809 (2000).

66. S.D. Park, M. Todo, K. Arakawa and M. Koganemaru, *Polymer*, **47**, 1357 (2006).

67. R.W. Nunes, J.R. Martin and J.F. Johnson, *Polymer Engineering & Science*, **22**, 205 (1982).

68. H. Bai, F. Luo, T. Zhou, H. Deng, K. Wang and Q. Fu, *Polymer*, **52,** 2351 (2011).

69. E. Lezak and Z. Bartczak, *Macromolecules*, **40**, 4933 (2007).

70. E. Lezak, Z. Bartczak and A. Galeski, *Macromolecules*, **39**, 4811 (2006).